geosciences

MDPI

Article

Sedimentary Diversity of Tsunami Deposits in a River Channel Associated with the 2024 Noto Peninsula Earthquake, Central Japan

Rina Okada [1,*], Koji Umeda [1], Keigo Motegi [2], Takanobu Kamataki [3] and Tadashi Amano [4]

[1] Graduate School of Science and Technology, Hirosaki University, 3 Bunkyo-cho, Hirosaki-shi 036-8561, Aomori, Japan; umeda@hirosaki-u.ac.jp
[2] Graduate School of Sustainable Community Studies, Hirosaki University, 3 Bunkyo-cho, Hirosaki-shi 036-8561, Aomori, Japan
[3] Faculty of Science, Okayama University of Science, 1-1 Ridai-cho, Kita-ku, Okayama-shi 700-0005, Okayama, Japan
[4] Electric Power Development Co., Ltd., 6-15-1 Ginza, Chuo-ku, Tokyo 104-8165, Japan
* Correspondence: r.okada@hirosaki-u.ac.jp

Abstract: A comprehensive analysis of modern tsunami deposits offers a valuable opportunity to elucidate the characteristics of paleo-tsunami deposits. On 1 January 2024, a tsunami was generated by a magnitude 7.6 seismic event and subsequently struck the Noto Peninsula in central Japan. In order to create a facies model of the tsunami deposits in terrestrial and riverine environments, field surveys were conducted on both the onshore and sandbars within the river channel in the Nunoura area on the northeastern Noto Peninsula. Terrestrial tsunami deposits were observed up to several hundred meters inland, with a slight decrease in thickness of several centimeters with distance from the shoreline. In terrestrial settings, the presence of a substantial silty layer overlying a graded sandy layer is indicative of ponded stagnant water from the tsunami wave. In contrast, riverine tsunami deposits are thicker and more extensive than terrestrial sediments, containing both gravels and shell fragments. An erosional surface develops between deposits of run-up and backwash flows, but a mud drape is not observed.

Keywords: tsunami deposits; the 2024 Noto Peninsula earthquake; river

check for updates

Academic Editors: Xingsen Guo, Dimitrios Nikolopoulos, Samuele Segoni, Danilo Godone, Giovanna Vessia and Leonhard Blesius

Received: 14 March 2025
Revised: 11 April 2025
Accepted: 12 April 2025
Published: 17 April 2025

Citation: Okada, R.; Umeda, K.; Motegi, K.; Kamataki, T.; Amano, T. Sedimentary Diversity of Tsunami Deposits in a River Channel Associated with the 2024 Noto Peninsula Earthquake, Central Japan. *Geosciences* **2025**, *15*, 153. https://doi.org/10.3390/geosciences15040153

Copyright: © 2025 by the authors. Licensee MDPI, Basel, Switzerland. This article is an open access article distributed under the terms and conditions of the Creative Commons Attribution (CC BY) license (https://creativecommons.org/licenses/by/4.0/).

1. Introduction

In contrast to the inundation of coastal areas by tsunamis, which typically reach several hundred meters inland, the penetration of tsunamis into rivers can extend much farther inland. This phenomenon has the potential to cause flooding in low-lying areas located several kilometers from the coastline [1]. Indeed, the 2011 Tohoku-oki tsunami overtopped a weir and penetrated 49 km up the Kitakami River, the fourth largest river in Japan [1]. Similarly, the 2010 Chile tsunami propagated at least 15 km up the Maule River [2].

On 1 January 2024, a magnitude 7.6 earthquake struck the western coast of Honshu Island, Japan, causing severe shaking along the Noto Peninsula (Figure 1). The earthquake, known as the 2024 Noto Peninsula earthquake, occurred at a depth of 15 km in the Noto Peninsula, followed by many aftershocks distributed across the peninsula in a NE–SW direction. The Geospatial Information Authority of Japan (https://www.gsi.go.jp/BOUSAI/20240101_noto_earthquake.html (accessed on 15 January 2024)) indicates that the rupture of active faults extended over an area of 102 km from west to northeast of the peninsula.

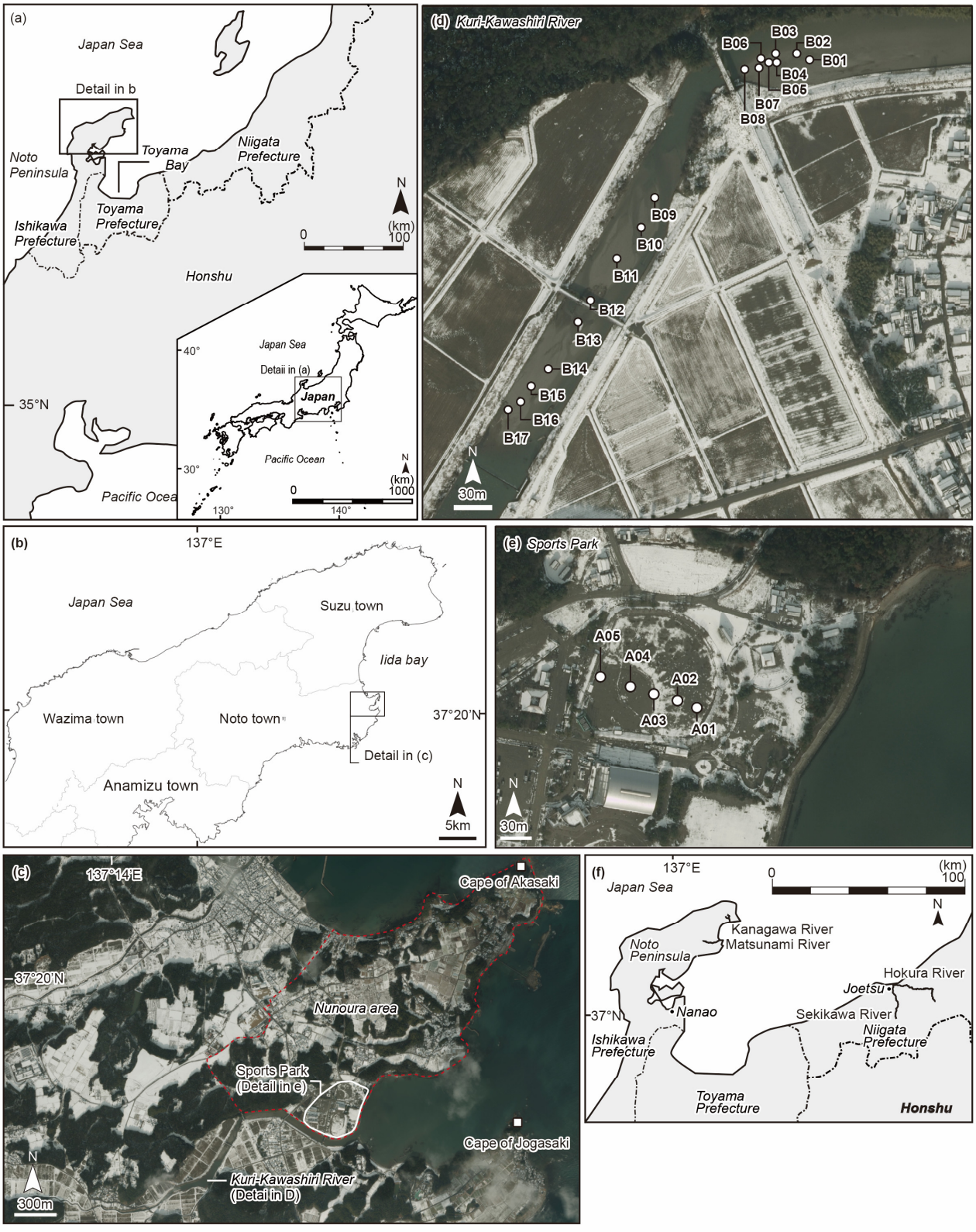


Figure 1. Location maps of the Noto Peninsula and collected samples. (**a**) Location of the Noto Peninsula in Japan. (**b**) Location map of the study area in Noto Peninsula. (**c**) Map of the area around the study site. The red dashed circle indicates the Nunoura area. (**d**,**e**) Sampling locations along Transects A and B. Aerial photos in panels (**c**–**e**) are from the Geospatial Information Authority of Japan (Taken on 14 January 2024, http://www.gsi.go.jp/BOUSAI/20240101_noto_earthquake.html#3-1 (accessed on 15 January 2024)). (**f**) Location map of four rivers. The Matsunami River and the Kanagawa River run through the towns of Suzu and Noto, respectively; the Sekikawa River and the Hokura River run through Joetsu City, Niigata Prefecture.

The earthquake triggered a tsunami that caused significant inundation along the coastal areas of the northeastern peninsula, subsequently propagating over the sea as rough wind waves and reaching the coast and rivers distant from the peninsula. The greatest inundation distance from the shoreline was observed in the Nunoura area, where an extensive lowland stretches along the Kuri-Kawashiri River. Tsunami traces indicate that the wave penetrated approximately 800 m inland from the coastline along a straight transect. Consistent with this wide-ranging propagation, traces of tsunami inundation were observed along the Shinhori River in Ishikawa Prefecture, located approximately 150 km from the epicenter, highlighting the extensive inland impact of the event [3]. The tsunami inundated over 1.90×10^6 m^2 of land in Ishikawa Prefecture and 4×10^4 m^2 in Niigata Prefecture (Figure 1a). Inundation and run-up heights were relatively high in the northeastern Noto Peninsula, reaching approximately 5.0 m, with high run-up values of ~7.0 m also observed in Niigata Prefecture. In contrast, the observed heights in the southeastern peninsula and Toyama Prefecture were low (Figure 1a) [4]. In Joetsu City, situated adjacent to the Noto Peninsula in Niigata Prefecture, the tsunami progressed up the Sekikawa River. This conclusion was corroborated by CCTV footage and wave and tide gauge data, which demonstrated that the tsunami propagated about 15 km from the river mouth. The inundation of the land situated between the Sekikawa and Hokura Rivers, near the mouth of the Sekikawa River, was observed as a result of the propagated tsunami originating from both rivers (Figure 1f). In some areas, the river embankments, which were over 3.0 m in height, were overtopped, resulting in the flooding of residential properties [5].

Tsunami deposits have been useful for estimating recurrence intervals and magnitudes of past tsunami waves [6,7]. Since the 1980s, paleo-tsunami deposits have been instrumental in elucidating ancient tsunami events (e.g., [8]). Nevertheless, the identification criteria and sedimentological characteristics of tsunami deposits were not well understood [9]. Recent events, such as the 2004 Indian Ocean and 2011 Tohoku-oki tsunamis, have provided valuable opportunities to study the sedimentary features and processes of modern tsunami deposits [10]. For example, the tsunami deposits left by recent tsunamis in low-lying coastal plains typically display a landward thinning and fining pattern (e.g., [11]). Although numerous studies have been conducted on sediments left behind by tsunami run-up on land, few studies have investigated sediments associated with tsunami propagation in rivers [12]. The sediments formed by tsunamis in riverine environments are subject to continuous modification by fluvial and eolian processes. As a consequence of both their susceptibility to continuous erosion and modification, as well as the inherent difficulties of undertaking such an investigation, the examination of tsunami deposits within rivers is a relatively uncommon procedure. For example, tsunami deposits that are formed within a river are difficult to discriminate from fluvial deposits.

The 2024 earthquake generated a tsunami that propagated through the Nunoura area of Noto Town on the northeastern peninsula facing Toyama Bay adjacent to Iida Bay, causing significant damage to coastal communities and infrastructure and resulting in the loss of more than 300 lives (Figure 1a,b). The study area comprises a valley with a lowland formed by alluvial deposits, through which the Kuri-Kawashiri River flows. The mouth of the river is a small bay between the capes of Jogasaki and Akasaki, which are about 2 km apart (Figure 1c). The post-tsunami foot and aerial surveys revealed not only tsunami deposits extending over 0.4 km inland from the coastline but also sediments carried by the tsunami wave deposited on sandbars about 1.2 km from the mouth of the Kuri-Kawashiri River (Figure 1c,d). The 2024 tsunami provides a unique opportunity to study the differences between the sedimentary facies of tsunami deposits in terrestrial and riverine environments.

The reconstruction of the hydraulic properties and magnitude of historical tsunamis from stratigraphic sequences can be a valuable tool in risk assessment studies. It should be noted, however, that event deposits in fluvial stratigraphic successions may also be produced by events such as storms and river flooding (e.g., [13]). As a result, it is important to investigate the detailed features of recent tsunami deposits from known source events. This is because their sedimentological characterization and relationship with the actual events are necessary for establishing the criteria to identify tsunami deposits in the geological record. The objective of this contribution is (a) to present the sedimentary structures of tsunami deposits associated with the 2024 earthquake in the Nunoura area, located on the northeast coast of the Noto Peninsula, (b) to establish a facies model of the tsunami deposits, both onshore and on sandbars within the river channel (Figure 1d,e).

2. Regional Setting

2.1. Geological Background

The Noto Peninsula is located on the west side of the Itoigawa-Shizuoka Tectonic Line (ISTL), central Japan, along which the North American Plate on the east side has been colliding with the Eurasian Plate on the west side since the beginning of Plio-Pleistocene time [14]. Exposed in the Noto Peninsula are widespread Late Oligocene to Early Miocene volcanic rocks and Late Miocene to Pliocene marine diatomaceous sediments ([15], Figure S1). The former rocks represent the rifting and spreading of the Japan Sea, and the latter represent the post-spreading thermal subsidence of the rift basin (e.g., [16]). The northern part of the peninsula is mainly composed of Neogene volcaniclastic and sedimentary rocks overlying Paleogene basement rocks. The study site, the Nunoura area, is situated on Holocene gravel, sand, and mud, overlying volcanic rocks of the early Miocene age (Kamiwazumi Formation, Horyuzan Formation). The Kamiwazumi formation is mainly composed of aphyric andesite lava flows, with reported ages of 23 to 20 Ma based on K–Ar dating. The Horyuzan Formation is composed of dacite volcaniclastic rocks, including siltstone, sandstone, and conglomerate, which were formed as a result of felsic volcanism that occurred between 19.5 and 18 Ma. Marine terraces developed on the Noto Peninsula during the Pleistocene, indicating long-term uplift of the land. The Kuri-Kawashiri River flows in an east–west direction through a lowland area surrounded by hills over 30 m in height composed of Late Pleistocene marine terrace deposits. The alluvial lowlands are utilized for rice paddy cultivation, with soil depths of about 0.2 m. The Kamiwazumi Formation is distributed upstream of the Kuri-Kawashiri River, whereas the Horyuzan Formation is extensively exposed along the coastline.

2.2. Tsunami Inundation

According to an aerial survey conducted by Ushiyama et al. in early February and March after the tsunami, the coastal lowlands from the northeastern to the eastern part of the Noto Peninsula were extensively inundated, with a maximum run-up distance of approximately 300 to 400 m from the coastline [17]. According to eyewitness accounts, tsunami waves ran up with debris for a distance of over 500 m along the narrow Hannya River within Iida Bay [18]. Notwithstanding the extensive damage caused by the earthquake and tsunami to water level gauges utilized in the flood monitoring system in rivers ([19] https://k.river.go.jp (accessed on 26 February 2024)), several gauges situated downstream of the river remained operational. The data provided by the water level measurements indicate that the tsunami waves ran up more than 1.2 km in the Matsunami River from the river mouth and more than 0.9 km in the Kanagawa River, facing Iida Bay (Figure 1f). These findings are consistent with the observation that the 2011 Tohoku-Oki tsunami exhibited the longest run-ups along rivers, with inundation distances reaching

three to four times greater than those occurring on the ground in the same area [20]. In the Nunoura area, post-tsunami aerial surveys revealed not only the extent of tsunami inundation, which reached 400 m inland from the coastline, but also the deposition of boats carried by the tsunami wave on river terraces about 1.5 km from the mouth of the Kuri-Kawashiri River.

3. Methodology

3.1. Field Survey

Field surveys were conducted on three separate occasions: 1–4 and 22–25 February, 2–7 April 2024. The inundation height was estimated by measuring the height of broken tree limbs, debris in trees, and watermarks on buildings. The inundation limit was determined by debris found piled up on the ground, and the run-up height was estimated by its elevation. Based on the evidence of fallen weeds and trees, it can be inferred that the waves advanced in a direction perpendicular to the coastline and reached about 0.7 km inland. The Nunoura area with tsunami propagation and inundation can be divided into two parts: the small coastal plain used as a sports park and the Kuri-Kawashiri River channel (Figure 2).



Figure 2. *Cont.*



Figure 2. Photographs of the field survey. (**A**,**B**) Photographs at the sports park, trees, and blocks have been washed away by the tsunami, and sand has been deposited on the ground. (**C**–**E**) Sandbars formed after the tsunami in Kuri-Kawashiri River. (**F**) Areas where the tsunami overflows the levee.

In the sports park, sediments were transported by the tsunami beyond the coastal seawall of approximately 2 m and covered the athletic fields in the sports park. The sedimentary structures of the tsunami deposit were investigated in two transects, which were surveyed using small pits. Transect A was established perpendicular to the shoreline on the athletic field situated on the coastal plain (Figure 1e). Transect B was arranged on sandbars that had formed along the river channel, located between 0.8 km and 1.2 km from the river mouth (Figure 1d). This study was conducted within the levee, with a focus on areas that were originally part of the river channel (Figure 2).

Tsunami deposits were observed at 5 locations along Transect A and 17 locations along Transect B. The study site locations were established using a GPS. At each observation site, erosional features and the distribution of tsunami sediments were examined, and pits were excavated to measure sediment thickness and depositional structures. To obtain samples from Transect B, a Handy Geoslicer sampling instrument (FUKKEN Co. Ltd., Hiroshima, Japan) was utilized to obtain a sample of subsurface tsunami deposits. The instrument is constructed from stainless steel and comprises a sample box and a shutter [21]. The extraction of the sample box and shutter results in the retrieval of an oriented sediment core measuring 0.1 m in width, 0.03 m in thickness, and 1.0 m in length. The undisturbed samples collected by the Handy Geoslicer enabled the observation of bed boundaries and sedimentary structures, as well as the vertical sections of the excavated trenches.

3.2. Sediment Descriptions

In the laboratory, plate-shaped plastic containers, which were 18 cm long, 7 cm wide, and 2 cm deep, were used at 8 locations to take samples for the soft-X imaging (Table 1), which was performed with a soft X-ray apparatus (M-60, Softex, Tokyo, Japan) and a digital X-ray sensor (NAOMI NX-06SN, RF Co., Nagano, Japan). Following the X-ray imaging, the sedimentary facies, sedimentary structures, grain size, and colors of each sample were described. Imaging was performed with settings of 3 mA and 40 kV, followed by image processing on software to conduct structural analysis. To achieve high-resolution analysis, the plastic container samples were subsequently sub-sampled vertically at 1 cm intervals for mineral assemblage and grain-size analyses. Subsampled sediment was wet-sieved using 63, 125, and 250 μm mesh sieves, and the residual grains were mostly <63 μm size fraction, and these were mounted on glass slides. The mineral composition and glass shard morphology were examined under the microscope.

Table 1. Positions of the surveyed locations along the transects and thickness of tsunami deposits measured at each location.

Transect A						
Location name	Distance from the coastline (m)	Grain-size analysis	Soft-X image	Thickness of tsunami deposits (cm)		
				Unit 1	Unit 2	**Total**
A01	117	○	-	4.5	1.0	**5.5**
A02	138	○	-	4.5	0.5	**5.0**
A03	160	○	-	5.0	0.5	**5.5**
A04	184	○	-	3.0	0.3	**3.3**
A05	213	○	-	3.0	0.5	**3.5**

Transect B							
Location name	Distance from the coastline (m)	Grain-size analysis	Soft-X image	Thickness of tsunami deposits (cm)			
				Unit 1	Unit 2	Unit 3	**Total**
B01	795	○	○	3	-	12	**15**
B02	824	-	-	11	-	1	**12**
B03	842	-	-	5	19	5	**29**
B04	848	-	-	-	15	-	**15**
B05	852	-	-	11	15	1	**27**
B06	859	○	○	7	11	4	**22**
B07	863	-	-	-	23	6	**29**
B08	870	○	○	12	-	29	**41**
B09	1000	-	-	-	-	51	**51**
B10	1020	-	-	-	-	30	**30**
B11	1060	○	○	-	-	28	**28**
B12	1100	○	○	-	-	14	**14**
B13	1120	-	-	2	-	20	**22**
B14	1160	○	○	-	15	15	**30**
B15	1180	○	○	-	10	23	**33**
B16	1190	-	-	-	19	18	**37**
B17	1200	○	○	11	-	44	**55**

3.3. Grain-Size Analysis

The grain size of the sediments was analyzed using laser diffraction with an effective measuring range of 0.1 to 2000 μm (SALD-3000J, SHIMADZU, Kyoto, Japan).

Samples comprised the tsunami deposit, the soil underlying the tsunami deposit, beach sand, and river sand. The core sample of the tsunami deposit was initially divided into 1 cm intervals. Prior to analysis, the organic matter was removed using hydrogen peroxide, and the sediments coarser than 2 mm were separated through sieving. The mean grain size and sorting of the grain-size distributions were calculated using the graphical methods proposed by [22].

3.4. Sedimentary Structure

Tsunami deposits identified at each site were classified into discrete sedimentary units following established sedimentological methodologies. This classification was carried out with high resolution and precision based on the following criteria: (1) the presence or absence of erosional contacts determined through detailed facies observations; (2) the occur-

rence of biogenic components such as shell fragments, plant debris, and wood fragments; (3) the identification of normal or inverse grading through grain-size distribution analysis; (4) variations in internal sedimentary structures as revealed by soft X-ray imaging; and (5) compositional differences in mineral assemblages.

4. Results

4.1. Transect A

In Transect A, excavations were conducted at 120 m and 250 m inland from the shoreline in order to observe the facies and collect samples. The height and direction of the watermarks and debris enabled us to estimate the flow depth and direction of the tsunami waves. The direction of Transect A was found to be consistent with that of the tsunami waves, and the flow depths were observed to be between 1.8 and 2.5 m above ground level around the transect. Debris was observed up to about 400 m inland from the shoreline.

The sedimentary structures observed in the pits indicated that the thickness of the tsunami deposits along Transect A ranged from 3.3 to 5.5 cm, with a slight decrease in sediment thickness with distance from the shoreline (Figure 3A). The tsunami deposits in the terrestrial environment were found to consist of two distinct sedimentary units, characterized by distinctive sedimentary structures and grain-size changes. These units are laterally traceable along Transect A. The lower unit directly overlies organic soil with an erosive boundary and contains abundant plant fragments derived from the underlying soil. It is composed mainly of well-sorted medium sand with a small amount of gravel. This unit is commonly massive and occasionally shows normal grading and/or faint parallel lamination (Figure 3B). Its thickness decreases landward from 3.0 to 5.0 cm. The upper unit is represented by a light gray massive silt layer with very fine sand, which ranges in thickness from 0.3 to 1.0 cm and covers the lower unit. The tsunami sediments in the lower unit contain minerals of 75% and volcanic glass shards of 16%. The mineral assemblage consists mainly of plagioclase associated with minor amounts of quartz and clinopyroxne. In contrast, the tsunami sediments in the upper unit comprise volcanic glass shards in a majority of 68%, with minerals representing 32% of the total content. The mineral assemblage is primarily composed of plagioclase, accompanied by minor quantities of quartz.

4.2. Transect B

In Transect B, sandbars were observed to have formed in the channel of the Kuri-Kawashiri River at two distinct locations, situated at distances of 790–870 m and 1000–1200 m from the river mouth, respectively. The tsunami propagation overflowed the right levee (1.95 m above sea level) at a distance of 800 m from the river mouth. Therefore, the tsunami height at this point can be estimated to be more than about 2.0 m asl. A total of 17 samples were obtained from tsunami deposits above sandbars along Transect B using the Handy Geoslicer. The thickness of the tsunami deposit decreased gradually from the river mouth, with a range of 12 to 55 cm. However, local variations in sediment thickness were observed in relation to topographic elevations of sandbars in the river channel. The observation of sedimentary features in each location revealed that the tsunami deposits within the river channel were composed of one to three sedimentary units, identifiable by distinctive sedimentary structures (Figure 4a), changes in grain size, and soft X-ray images (Figure 4b). Each sedimentary unit was identified in the tsunami deposit along Transect B and is bounded by either a sharp erosive surface or distinctive grain-size change.

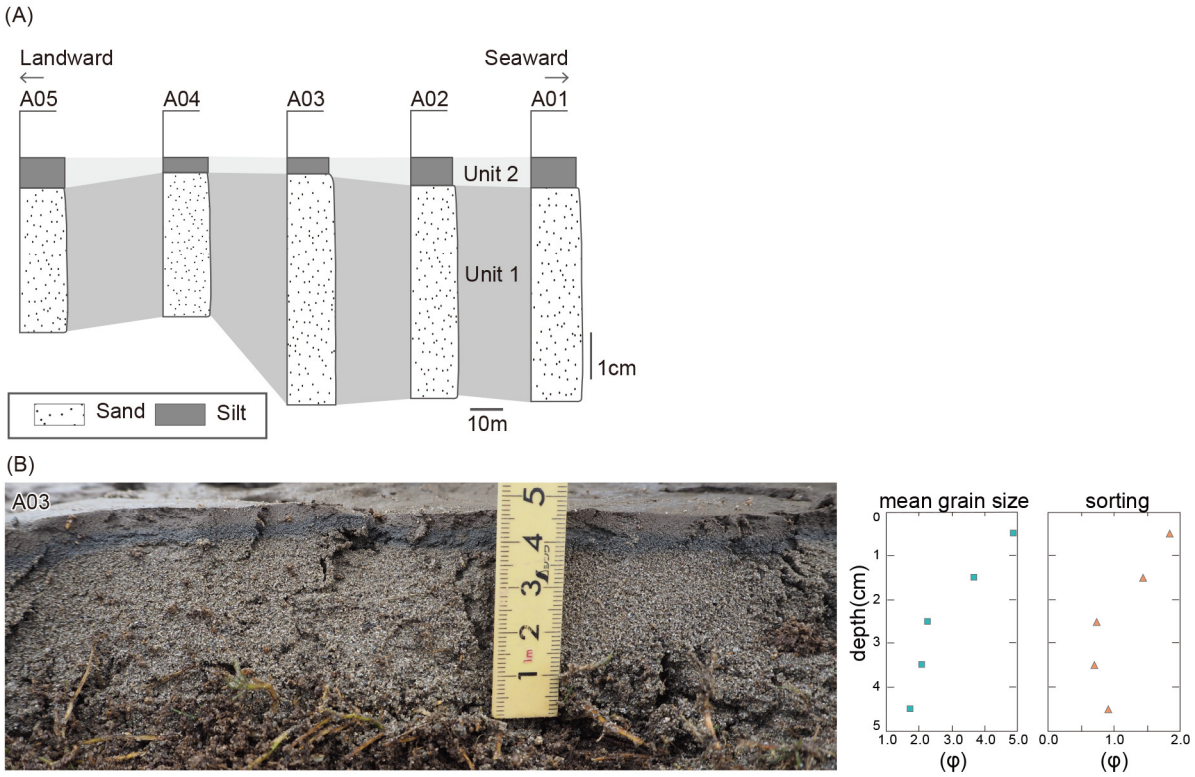


Figure 3. (**A**) Sedimentary columns along the survey Transect A and correlations of the two sedimentary units between sampling locations (locations in Figure 1e). (**B**) Photograph of the tsunami deposit at A03 and graphs showing vertical changes in mean grain size and sorting.

Unit 1, the lowest unit, directly overlies sandbars comprising black soil and silt at locations B01–03, 05, 06, 08, 13, and 17, with an erosive boundary. It is mainly composed of dark gray coarse to medium sand, containing a high abundance of shell, shell fragments, fluvial gravels, and mud clasts. Unit 1 deposits are found to contain gravels comprising more than 5% of their composition. The unit ranges from 2 to 12 cm in thickness. This unit is overlain by either Unit 2 or Unit 3. Inverse grading is a relatively common occurrence in this unit. The tsunami sediments in Unit 1 contain 84% minerals and 16% volcanic glass shards. The mineral assemblage consists mainly of plagioclase associated with minor amounts of orthopyroxene and quartz.

Unit 2 deposits are composed of reddish-brown, well-sorted very coarse to coarse sand and are distributed at locations B03–07, 14–16, with a thickness ranging from 10 to 23 cm. The grain-size analysis indicates that the deposits are characterized by normal grading. The microstructure of these deposits is comparable to that observed in fluvial gravels and pumice clasts within the river channel. This unit frequently exhibits sedimentary structures indicative of a backwash current, such as current ripple cross-lamination. The tsunami sediments in Unit 2 comprise minerals in a majority of 92%, with volcanic glass shards representing 8% of the total content. The mineral assemblage is primarily composed of plagioclase, accompanied by minor quantities of quartz, ilmenite, and alkali feldspar.

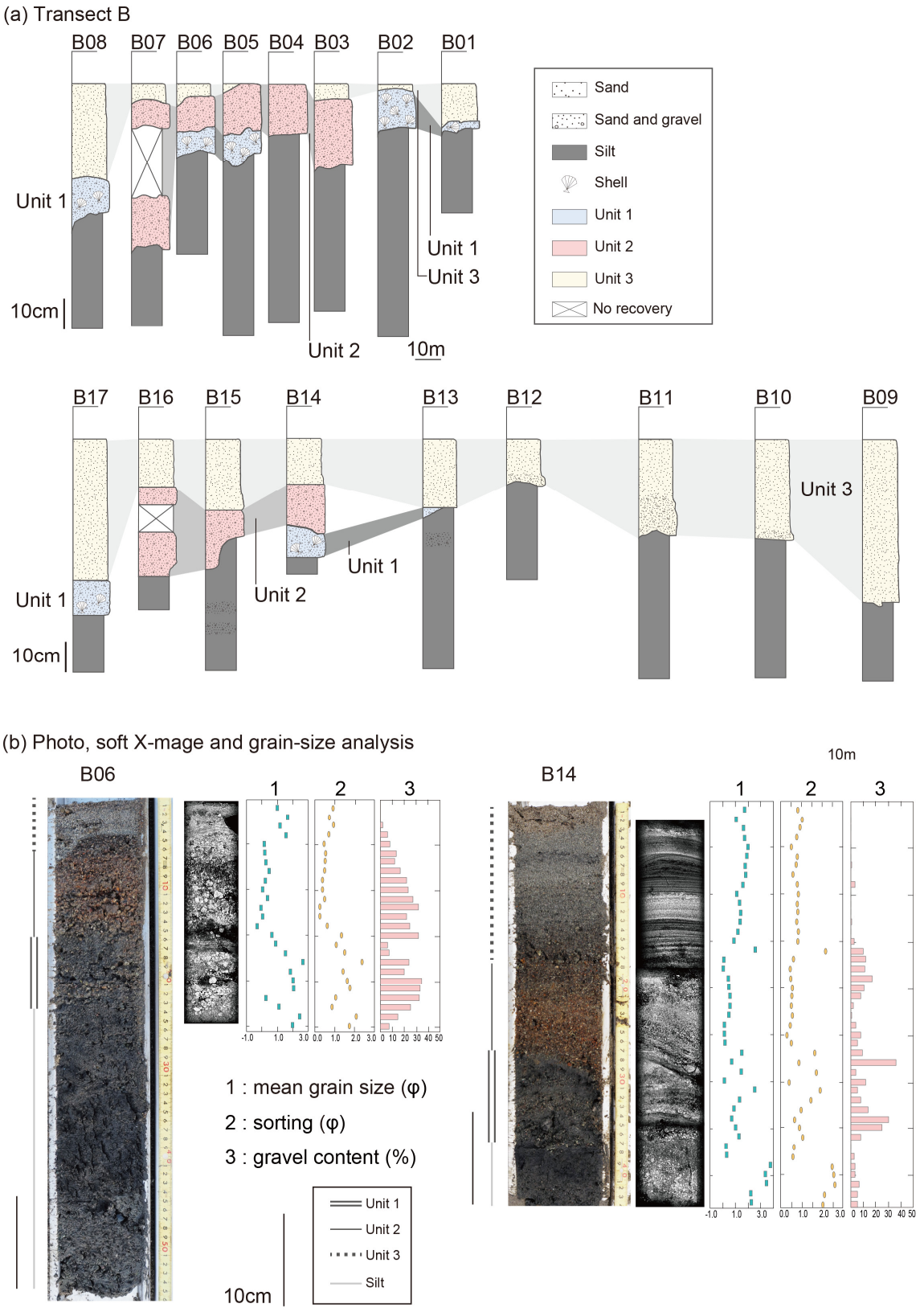


Figure 4. (**a**) Sedimentary columns along the survey Transect B and correlations of the three sedimentary units between sampling locations (locations in Figure 1d). (**b**) Photograph, a soft X-image, and graphs showing vertical changes in mean grain size, sorting, and gravel content (excluding at B15) at locations B06 and B14.

Unit 3 deposits are distributed across all locations with the exception of B04; furthermore, the lower units or sandbars are overlaid with an erosional boundary. This unit is characterized by light gray sand-sheet facies, comprising predominantly fine to medium sand, containing shell fragments. The thickness of Unit 3 deposits ranged from 1 to 51 cm. The unit is identified by characteristics indicative of normal grading. The deposits that directly overlie sandbars frequently include rip-up clasts derived from black soil or silt. The sedimentary facies typically exhibit a lower zone with parallel lamination and an upper zone with wave ripple cross-lamination, as evidenced by soft X-ray analyses. The current ripple lamination observed at the top of Unit 3 indicates a unidirectional flow oriented landward. Conversely, a seaward flow direction is also rare. The tsunami sediments in Unit 3 contain 83% minerals and 17% volcanic glass shards. The mineral assemblage consists mainly of plagioclase associated with minor amounts of quartz.

The sedimentary units of the tsunami deposit examined in this study exhibit notable lateral variation in terms of both thickness and sedimentary structures. Unit 3 is distinguished by its relatively extensive distribution, with a nearly constant thickness except for the point bar form found on the inner side of meander bends in the river. In contrast, Units 1 and 2 are characterized by their limited spatial distribution, with the whole succession of these units observable only in three cored locations. In addition to the sandy tsunami deposits, several boulders were identified within the river channel. The boulder, which had transported the sandbar at a distance of 800 cm from the river mouth, had a diameter of over 130 cm. These boulders were composed of volcanoclastic sediments, including pumice clasts and epiclastic sediment blocks of varying sizes. The mouth of the river was observed to have a freshly collapsed outcrop, which was identified as the likely source of the boulders [23].

5. Discussion and Conclusions

5.1. Sedimentary Diversity of Tsunami Deposits in the Kuri-Kawashiri River

In order to prevent flooding, the Kuri-Kawashiri River was widened, and a dam was constructed upstream in the 1960s. Consequently, a sandbar consisting mainly of black sediment and mud, rather than sand and gravel, was formed along the river bank in the widened area up to the river mouth. As illustrated in Figure 5, prior to the widening of the river channel, the floodplain was outside the channel. The findings indicate that the tsunami that propagated upstream of the river resulted in the formation of tsunami deposits on the sandbars, which may be largely resistant to significant fluvial processes, including subsequent erosion and deposition.

Prior to and following the tsunami triggered by the 2024 earthquake, the river mouth of the Kuri-Kawashiri River exhibited a range of morphological alterations. The river mouth sediments that accumulated up to about 200 m upstream from the mouth before the tsunami were eroded and transported upstream by the intruding waves (Figure 6). The tsunami deposits observed in the river channel are thought to have originated predominantly from the river mouth sediments (fluvial sand and gravel), in addition to marine sediments (well-sorted sand with shell fragments).

Unit 1 deposits are composed of coarse to medium sand, containing a high abundance of shell fragments and fluvial gravels. They are characterized by very poor sorting, indicating that the initial tsunami propagation in the river transported the river mouth and marine sediments by traction. The sedimentary structures, which are composed of detrital sediments derived from both coastal and fluvial environments, are regarded as distinctive formations attributable to the tsunami run-up in the river. In addition, inverse grading is commonly observed in Unit 1. The shear velocity of the run-up current of the tsunami reduces with increasing distance from the source, such that even temporally increasing flows can accumulate the inversely graded beds [24].



Figure 5. Photographs of the changes in river width in the Kuri-Kawashiri River, widened in the 1960s. (**A**) Before widening. (**B**) After widening. Aerial photos in panels (**A**,**B**) are from the Geospatial Information Authority of Japan (MCB676X-C8-27 and CB812X-C8-29).

The deposits of Unit 2 are predominantly composed of well-sorted, very coarse to coarse sand, which is extensively deposited on the riverbed. These deposits are distinguished by normal grading. Unit 2 directly overlies sandbars or Unit 1 with an erosive boundary. As mentioned above, current ripple lamination that indicates a seaward flow direction can be observed at the bottom of Unit 2. It is possible that the Unit 2 deposits were formed as a result of the backwash current associated with the initial propagation of the tsunami within the river channel. In general, the backwash currents of the tsunami run through complex pathways, concentrating in topographical lows and depositing thinner beds [25]. However, in riverine settings, the backwash current deposits may be significantly more extensive and thicker. In addition, although stagnant water exists in the terrestrial setting during the turnover phase from the run-up to the backwash current, in a riverine setting where there is constant flow, there is no time for water to stagnate. Therefore, mud drapes formed by stagnant water are found in terrestrial settings and do not form in riverine settings. As a result, a mud drape does not develop at the top of the run-up current deposits in the riverine setting.

Unit 3 is characterized by normal grading. The occurrence of graded bedding is frequently ascribed to deposition from suspension fallout under stagnant water conditions (e.g., [26]). However, the graded bedding observed in the Kuri-Kawashiri River frequently exhibits parallel lamination, which is indicative of bedload transport of sediments [27]. Masuda et al. (2024) [28] examined tsunami propagation and inundation processes by comparing simulations with available observations to depict the general characteristics of the tsunami source. A tsunami propagation and inundation model estimated that the coastal area of Iida Bay was inundated to a maximum depth by the second wave. Although the initial wave did not contribute to inundation in the coastal area, the tsunami propagated into the Kuri-Kawashiri River. As mentioned above, the grain-size distribution and mineral composition of the onshore tsunami deposits and riverine Unit 3 exhibit notable similarities, indicating that they were derived from a common source. Consequently, it can be inferred that both sediments were transported by the second wave, which arrived approximately 30 min after the earthquake.



Figure 6. Changes of sandbars in Kuri-Kawashiri River before (**B**) and after the Noto Peninsula earthquake. Change in sandbar at sampling sites (**A**). Change in sandbars at the mouth of an estuary. The solid boxes indicate the areas of (A) and (B), while the dashed circles indicates the sandbar. Aerial photos in panels are from the Geospatial Information Authority of Japan (After the tsunami: Taken on 14 January 2024, Before the tsunami: CCB-2010-1X-C12-30).

5.2. Discrepancies Between Sedimentary Structures of Tsunami Deposits in Terrestrial and Riverine Settings

The second tsunami wave generated by the 2024 Noto Peninsula earthquake inundated the Nunoura area, resulting in the formation of tsunami deposits in terrestrial and riverine settings. Terrestrial tsunami deposits were observed to reach a maximum distance of approximately 400 m inland from the shoreline. The maximum recorded thickness was 5.5 cm; however, a slight decrease in sediment thickness was observed with distance from the shoreline. In the case of the run-up current in terrestrial settings, ponded stagnant water of the tsunami wave probably formed the massive silty bed that drapes the graded sandy bed. The sediments are characterized by the presence of shell fragments, but there is an absence of fluvial gravels.

In contrast, the occurrence of riverine tsunami deposits (Unit 3) was inferred to have occurred at a distance of more than 1200 m from the river mouth, with inland invasion extending up to three times farther than in terrestrial areas. The distribution of riverine tsunami deposits is more extensive and of greater thickness than that of terrestrial sediments. The sediments contain both fluvial gravels and shell fragments. The second wave resulted in extensive

erosion of the deposit of Units 1 and 2 formed by the initial wave, suggesting that the flow velocity of the second wave was greater than that of the first wave.

Supplementary Materials: The following supporting information can be downloaded at: https://www.mdpi.com/article/10.3390/geosciences15040153/s1, Figure S1: Positions of the surveyed locations along the transects and thickness of tsunami deposits measured at each location.

Author Contributions: Formal analysis, R.O. and K.M.; investigation, R.O., K.M. and K.U.; writing—original draft preparation, R.O.; writing—review and editing, K.U., T.K. and T.A. All authors have read and agreed to the published version of the manuscript.

Funding: This research received no external funding.

Data Availability Statement: The aerial photo data utilized in this research were obtained from the Geospatial Information Authority of Japan (https://www.gsi.go.jp/ (accessed on 15 January 2024)). No new or additional data were generated or analyzed for the other aspects of this research.

Acknowledgments: We are grateful to three anonymous reviewers for their comments, which were very helpful in improving the manuscript. This work was partially supported by grants from the Graduate School of Sustainable Community Studies, Hirosaki University for the 2024 Noto Peninsula Earthquake Project.

Conflicts of Interest: Author Tadashi Amano was employed by the company Electric Power Development Co., Ltd. The remaining authors declare that the research was conducted in the absence of any commercial or financial relationships that could be construed as a potential conflict of interest.

References

1. Tolkova, E.; Tanaka, H. Tsunami Bores in Kitakami River. *Pure Appl. Geophys.* **2016**, *173*, 4039–4054. [CrossRef]
2. Fritz, H.M.; Petroff, C.M.; Catalán, P.A.; Cienfuegos, R.; Winckler, P.; Kalligeris, N.; Weiss, R.; Barrientos, S.; Meneses, G.; Valderas-Bermejo, C.; et al. Field Survey of the 27 February 2010 Chile Tsunami. *Pure Appl. Geophys.* **2011**, *168*, 1989–2010. [CrossRef]
3. Tajima, Y.; Matsuba, Y.; Yamanaka, Y.; Shimazono, T.; Kato, F. Estimation of tsunami characteristics under rough wind waves in the 2024 Noto Peninsula Earthquake. *Coast. Eng. J.* **2024**, *66*, 419–433. [CrossRef]
4. Yuhi, M.; Umeda, S.; Arita, M.; Ninomiya, J.; Gokon, H.; Arikawa, T.; Baba, T.; Imamura, F.; Kumagai, K.; Kure, S.; et al. Post-event survey of the 2024 Noto Peninsula earthquake tsunami in Japan. *Coastal Eng. J.* **2024**, *66*, 405–418. [CrossRef]
5. Yuhi, M.; Umeda, S.; Arita, M.; Ninomiya, J.; Gokon, H.; Arikawa Baba, T.; Imamura, F.; Kumagai, K.; Kure, S.; Miyashita, T.; et al. Dataset of Post-Event Survey of the 2024 Noto Peninsula Earthquake Tsunami in Japan. *Sci. Data* **2024**, *11*, 786. [CrossRef] [PubMed]
6. Goff, J.; Chagué-Goff, C.; Nichol, S.; Jaffe, B.; Dominey-Howes, D. Progress in palaeotsunami research. *Sediment. Geol.* **2012**, *243*, 70–88. [CrossRef]
7. Jaffe, B.E.; Gelfenbuam, G. A simple model for calculating tsunami flow speed from tsunami deposits. *Sediment. Geol.* **2007**, *200*, 347–361. [CrossRef]
8. Atwater, B.F. Evidence for great Holocene earthquakes along the outer coast of Washington state. *Science* **1987**, *236*, 942–944. [CrossRef]
9. Shanmugam, G. Process-sedimentological challenges in distinguishing paleo-tsunami deposits. *Nat. Hazards* **2012**, *63*, 5–30. [CrossRef]
10. Goto, K.; Chagué-Goff, C.; Goff, J.; Jaffe, B. The future of tsunami research following the 2011 Tohoku-oki event. *Sediment. Geol.* **2012**, *282*, 1–13. [CrossRef]
11. Fujino, S.; Naruse, H.; Matsumoto, D.; Sakakura, N.; Suphawajruksakul, A.; Jarupongsakul, T. Detailed measurements of thickness and grain size of a widespread onshore tsunami deposit in Phang-nga Province, southwestern Thailand. *Isl. Arc.* **2010**, *19*, 389–398. [CrossRef]
12. Oota, K.; Sagayama, T.; Inui, T.; Hoyanagi, K. Depositional process in response to waveform of the 2011 Tohoku oki tsunami inundated the Atsuma gawa River in Hokkaido, Northern Japan. *J. Geol. Soc. Jpn.* **2017**, *123*, 551–566. [CrossRef]
13. Switzer, A.D.; Jones, B.G. Large-scale washover sedimentation in a freshwater lagoon from the southeast Australian coast: Sea-level change, tsunami or exceptionally large storm? *Holocene* **2008**, *18*, 787–803. [CrossRef]
14. Kato, H. FOSSA MAGNA—A masked border region separating southwest and northeast Japan. *Bull. Geol. Surv. Jpn.* **1992**, *43*, 1–30.
15. Geological Survey of Japan; AIST. Seamless Digital Geological Map of Japan V2 1:200,000 [Dataset]. 2022. Available online: https://gbank.gsj.jp/seamless/ (accessed on 15 January 2024).

16. Ozaki, M. 1:200,000 Geological Map of the Northern Part of Noto Peninsula. In S-1. Seamless Geoinformation of Coastal Zone "Northern Coastal Zone of Noto Peninsula". 2010, p. 13. Available online: https://www.gsj.jp/data/coastal-geology/GSJ_DGM_S1_2010_02_b.pdf (accessed on 15 January 2024).
17. Ushiyama, M.; Sugamura, K.; Yokomaku, S. Tsunami Casualties Caused by the Noto Peninsula Earthquake of 2024. *J. JSNDS* **2024**, *43*, 187–206, (In Japanese with English Abstract)
18. Shimada, Y.; Matsumoto, D.; Tanigawa, K.; Sawai, Y. Sedimentological and micropaleontological characteristics of tsunami deposits associated with the 2024 Noto Peninsula earthquake. *Sci. Rep.* **2024**. submitted. [CrossRef]
19. The Flood Monitoring System in Rivers. Available online: https://k.river.go.jp (accessed on 26 February 2024).
20. Liu, H.; Shimozono, T.; Takazawa, T.; Okayasu, A.; Fritz, H.M.; Sato, S.; Tajima, Y. The 11 March 2011 Tohoku Tsunami Survey in Rikuzentakata and Comparison with Historical Events. *Pure Appl. Geophys.* **2013**, *170*, 1033–1046. [CrossRef]
21. Takada, K.; Atwater, B.F. Evidence for Liquefaction Identified in Peeled Slices of Holocene Deposits along the Lower Columbia River, Washington. *Bull. Seismol. Soc. Am.* **2004**, *94*, 550–575. [CrossRef]
22. Folk, R.L.; Ward, W.C. Brazos River bar; a study in the significance of grain size parameters. *J. Sediment. Res.* **1957**, *27*, 3–26. [CrossRef]
23. Yamada, M.; Naruse, H.; Ishimura, D.; Nakanishi, R.; Maehashi, K.; Kiyozuka, Y. Tsunami deposits formed in Suzu City and Noto Town by the 2024 Noto Peninsula earthquake. In Proceedings of the Japan Geoscience Union Meeting 2024, Chiba, Japan, 26–31 May 2024. U15-P73, abstract.
24. Choowong, M.; Murakoshi, N.; Hisada, K.; Charusiri, P.; Charoentitirat, T.; Chutakositkanon, V.; Jankaew, K.; Kanjanapayont, P.; Phantuwongraj, S. 2004 Indian Ocean tsunami inflow and outflow at Phuket, Thailand. *Mar. Geol.* **2008**, *248*, 179–192. [CrossRef]
25. Umitsu, M.; Tanavud, C.; Patanakanog, B. Effects of landforms on tsunami flow in the plains of Banda Aceh, Indonesia, and Nam Khem, Thailand. *Mar. Geol.* **2007**, *242*, 141–153. [CrossRef]
26. Kon'no, E. (Ed.) *Geological Observation of the Sanriku Coastal Region Damaged by the Tsunami Due to the Chile Earthquake in 1960*; Contribution of Institute of Geology and Paleontology, Tohoku University: Sendai, Japan, 1961; Volume 52, pp. 1–45, (In Japanese with English Abstract)
27. Bridge, J.S.; Best, J.L. Flow, sediment transport and bedform dynamics over the transition from dunes to upper-stage plane beds: Implications for the formation of planar laminae. *Sedimentology* **1988**, *35*, 753–763. [CrossRef]
28. Masuda, H.; Sugawara, D.; Cheng, A.; Suppasri, A.; Shigihara, Y.; Kure, S.; Imamura, F. Modeling the 2024 Noto Peninsula earthquake tsunami: Implications for tsunami sources in the eastern margin of the Japan Sea. *Geosci. Lett.* **2024**, *11*, 29. [CrossRef]

Disclaimer/Publisher's Note: The statements, opinions and data contained in all publications are solely those of the individual author(s) and contributor(s) and not of MDPI and/or the editor(s). MDPI and/or the editor(s) disclaim responsibility for any injury to people or property resulting from any ideas, methods, instructions or products referred to in the content.